Rate Coefficient Measurements of the Reaction $CH_3 + O_2 = CH_3O + O$

S. M. Hwang, Si-Ok Ryu,† and K. J. De Witt

Department of Chemical Engineering, The University of Toledo, Toledo, Ohio 43606

M. J. Rabinowitz*

National Aeronautics and Space Administration, Glenn Research Center at Lewis Field, Cleveland, Ohio 44135

Received: March 23, 1999; In Final Form: June 4, 1999

Rate coefficients for the reaction $CH_3 + O_2 = CH_3O + O$ were measured behind reflected shock waves in a series of lean CH_4-O_2-Ar mixtures using hydroxyl and methyl radical diagnostics. The rate coefficients are well represented by an Arrhenius expression given as $k = (1.60^{+0.67}_{-0.47}) \times 10^{13} \exp(-15813 \pm 587\ K/T)$ $cm^3\ mol^{-1}\ s^{-1}$. This expression, which is valid in the temperature range 1575−1822 K, supports the downward trend in the rate coefficients that has been reported in recent determinations. All measurements to date, including the present study, have been to some extent affected by secondary reactions. The complications due to secondary reactions, choice of thermochemical data, and shock−boundary layer interactions that affect the determination of the rate coefficients are examined.

Introduction

Methyl radical is formed rapidly during the preignition phase in the combustion of nearly all hydrocarbons. It is relatively unreactive and is consumed only slowly until a large population of reactive radicals, such as O atoms or hydroxyl radicals, is encountered. In a flame this necessitates transport through space to either a hotter or leaner region, and in a shock tube it requires, in essence, transport through time. The radical−radical reactions that then ensue are rapid, exothermic, and chain-propagating. An exothermic and chain-propagating reaction is also possible between methyl radical and molecular oxygen. Such a reaction, and indeed any methyl radical−molecular oxygen reaction, would effectively control the flow of reaction during the radical-starved preignition phase. Important characteristics of flame propagation and ignition behavior are governed by the flow of reaction in the preignition phase, and so both the rate and products of such a reaction would be attractive subjects for speculation and experimental evaluation. And so they have been.

Early studies of hydrocarbon oxidation, concerned mainly with the overall structure of the reaction mechanism, were performed using methane as a representative and experimentally amenable fuel.[1−11] The accepted oxidation pathway for methyl radical during the preignition phase was the chain-propagating reaction $CH_3 + O_2 = CH_2O + OH$. This is an exothermic reaction ($\Delta_r H°_{298} = 286.6$ kJ mol^{-1}) that must proceed via a four-center multiple bond rearrangement and so should be expected to proceed slowly. However, the reported rate coefficient values were unexpectedly high (and much higher than are currently accepted). There were good reasons for this. The early researchers did not yet recognize the sweeping complexity of the methane oxidation mechanism; their mechanisms contained only 16−23 reaction steps. This led them to believe that they had achieved chemical isolation, i.e., a system in which the target reaction alone controls the measured characteristics. Also, and of equal importance, rapid growth of chain carriers was attained in the early mechanisms through the chain-branching reaction $H + O_2 = OH + O$, which, at the time, was believed to be very fast. That belief was challenged by Schott,[12] who in 1973, established a rate coefficient about half the then accepted value. It soon became clear that another reaction would be needed to provide sufficient chain branching in methane oxidation. An obvious source of chain branching is the reaction channel $CH_3 + O_2 = CH_3O + O$. These two chain-branching reactions are analogous; both are endothermic radical−molecule reactions that increase the chain carrier number and increase the free valence number. The dominance of the chain-branching channel was demonstrated in the 1974 study of Brabbs and Brokaw[13] that examined the growth of the radical pool in methane oxidation. They proposed the title reaction as the only possible explanation of their measurements. Since that time the reaction rate and products have been the subject of various studies. In general the dominance of the chain-branching channel at combustion temperatures was upheld,[8,14−24] although some studies[25,26] have indicated that the chain-propagating channel was dominant. Various levels of theoretical studies have been performed[26−28] with nearly all supporting the dominance of the chain-branching channel.

The relative importance of the two product channels still remains at issue. Published experimental rate coefficient expressions for the chain-propagating channel, evaluated at 1600 K, span a factor of 19, while the expressions for the chain-branching channel span a factor of 6 at that temperature. The reported values of the chain-branching reaction at 1600 K have declined with the passage of time in a manner that is more or less sinuosoidal. This trend has not been decisive, and the large uncertainty is unacceptable for such an important reaction. The general decline is, in part, a result of the increasing sophistication evident in kinetic modeling arising from a growing appreciation of the role of secondary reactions. It is our belief that secondary reaction chemistry plays a significant role in the discrepancy

* To whom correspondence should be addressed. E-mail marty@grc.nasa.gov.

† Permanent address: School of Chemical Engineering and Technology, Yeungnam University, Kyongsan, Korea.

10.1021/jp990998o CCC: $18.00
Published on Web 07/09/1999

between the various rate coefficient determinations that has motivated us to reinvestigate the title reaction.

Experimentalists have exploited a plethora of diagnostics for studies of the title reaction covering a broad range of mixtures and conditions.[13,15−25,29] As always, a compromise has been made between experimental convenience and chemical isolation. We have also made such a compromise in our study, permitting, over a somewhat narrow temperature range, fruitful application of our experimental apparatus and analytical techniques. All experiments were performed behind reflected shock waves in lean CH_4-O_2-Ar mixtures using two different optical diagnostics. The rate coefficients were derived by matching characteristic times obtained from absorption profiles of methyl radical at ca. 214 nm and hydroxyl radical at ca. 310 nm.

Experimental Section

A rolled-square stainless steel shock tube with a cross sectional diameter of 63.5 mm was used for all experiments. Before each run the test section was routinely pumped to 3 μTorr using a Varian V60 turbopump. All shocks were initiated within 1 min of admitting the test gas mixture. Gas mixtures were prepared manometrically and allowed to stand at least 48 h before use. Maximum uncertainty in mixture composition was less than 0.5% of the nominal mole fraction for each component. The stated purities of the gases were the following: CH_4, 99.999%; O_2, 99.999%; Ar, 99.9999%. All gases were used without further purification.

Optical access was provided via two 25.4 mm S1-UVA windows flush-mounted with the interior walls of the shock tube. Shock velocities were measured using a series of flush-mounted 113A21 PCB Piezotronics pressure transducers coupled to Phillips PM6666 programmable counter−timers. One pressure transducer was axially coincident with the center of the observation windows, 12.7 mm distant from the end wall. Reflected shock conditions were derived from incident shock velocities in a three-step process. First, velocities were fitted to a second-order polynomial in distance. Next, the velocity, extrapolated to the end wall, was used to solve the standard shock relationships, assuming full vibrational relaxation and no chemical reaction at the shock front. Finally, the computed shock properties were corrected for boundary layer interaction effects in a fashion similar to the method of Michael and Sutherland.[30] The postshock pressure, needed for the boundary layer correction, was measured using the pressure transducer centered above the windows. Pressure transducers were calibrated, in their mounting assemblies, at the NASA Glenn Research Center Calibration Laboratory.

Two separate optical diagnostics were employed. Light at ca. 214 nm, absorbed mainly by methyl radical and molecular oxygen, was produced using a BHK, Inc. Premier zinc lamp run in dc mode. Light at ca. 310 nm, $P_1(5)$ line of the (0,0) band of the OH $A^2\Sigma^+-X^2\Pi$ transition, was produced using a CW laser pumped doubled ring dye-laser apparatus, which, in our case, was a Coherent Innova 200 CW argon ion laser pumping a Coherent 899-21 ring dye-laser running Kiton Red 620 dye with intracavity frequency doubling achieved using an angle-tuned $LiIO_3$ crystal. The usual paraphernalia were employed for both light sources. The 214 nm light was passed through a collimating lens before entering the shock tube. A 2 mm slit was placed over the exit window to both enhance time resolution and reduce emission from the shock-heated gases (plausibly CO fourth positive band). The detector was an interference filter−PMT−buffer combination comprised of a 214 nm interference filter (10 nm fwhm), a Thorn EMI 9924QB PMT, and a custom high-speed buffer−amplifier circuit used to isolate the anode from the signal cables. The distance from the shock tube to the detector was 1.0 m to minimize emissions from within the shock tube falling onto the detector. At distances below 0.5 m, emission from the shock-heated gases became observable. At distances below 0.25 m, the emission sufficiently modified the signal to corrupt the interpretation of the signal. When placed adjacent to the shock tube window, the maximum emission intensity was significantly greater than the lamp intensity for all of our mixtures. The broad emission signal was found to peak approximately at the same time as the maximum pressure rise, which occurred slightly after the maximum 214 nm absorption. This strong emission modified the experimental trace by shortening the apparent time to peak absorption and so shortening the ignition characteristics measured on the basis of peak absorption (see Results below). Rate coefficients reduced from such corrupted data would manifest spuriously high values.

A standard three-path configuration was used for the 310 nm laser light: a signal beam passed through the shock tube and then onto a detector, an intensity reference beam passed directly onto a detector, and a wavelength reference beam passed through a burner-stabilized methane−air flame (used to determine the line center of the hydroxyl absorption feature). The detectors were similar to that used in the 214 nm experiment with the obvious change in the interference filter, now centered at 310 nm (10 nm fwhm). A less obvious but equally important change was the replacement of the full 11 dynode configuration in the PMT with a custom configuration using only five dynodes to ensure full optical response and linearity for the higher light flux. Use of the standard dynode chain and the recommended interdynode potentials, required for proper electron optics, would have led, at our high light intensity levels, to a situation where the anode current would have vastly exceeded 10% of the dynode current. Above that level it is generally accepted that PMT performance is degraded, resulting in a loss of linearity and optical response, i.e., a lower apparent absorption.[31] Verification of the linearity and optical response of our detectors was achieved via calibration using a set of Melles Griot neutral density filters that, at 310 nm, covered the range 0.337−2.12 in optical density (OD). The overall electronic time constant determined for the entire PMT−buffer−cable system for both sets of experiments was less than 0.5 μs.

Selection of Experimental Conditions and Computer Simulation

Simulation of the experimental profiles was performed using three different computer codes as was appropriate. Chemkin II[32] and LSENS[33] are widely available chemical kinetics codes, and the third is a custom code based on the LSODE[34] integrator, which has built-in features beneficial for optimization. Indistinguishable results were obtained using the three codes for a series of calculations with GRI_MECH, version 2.11,[35] and either NASA thermodynamic data[36] or GRI_thermodynamic data, version 2.11.[35]

Extensive sensitivity analyses were performed to determine optimum mixtures and conditions for our diagnostics. When chemical isolation cannot be achieved, as has so far been the case for the study of the title reaction, the rate coefficients of the trial reaction mechanism used in the sensitivity analysis must be critically examined. Yu et al.[23] (YWF) published a sensitivity study for the title reaction that demonstrated dominant sensitivity for the OH profile at 1600 K in a lean CH_4-O_2-Ar mixture. However, their measured value for the rate coefficient at that temperature was 1.5 times smaller than the value they used in

their sensitivity study. Subsequently, Braun-Unkhoff et al.[24] (BNF) measured the rate coefficients for the title reaction and reported an expression that at 1600 K was about half the YWF value. Therefore, on the basis of the experimental results of BNF and our observation that the rate coefficient has been generally diminishing over time (see Introduction above), we reduced the rate coefficient expression used by YWF in their sensitivity study by a factor of 3 in our sensitivity analysis. This resulted in a restriction of the experimentally useful temperature range as explained below. It is always worthwhile to remember that sensitivity analysis is a procedure that results in the local measurement of the response gradient at an arbitrarily defined location in the parameter space no matter how adeptly enacted. We are constrained in our choice of location in parameter space to those that are currently held to be physically realistic. All other reactions in the GRI_MECH, version 2.11, were used unchanged.

For the selection of mixture composition, sensitivities to characteristic times (defined in Results below) for the two available diagnostics, 310 nm OH absorbance and 214 nm methyl radical absorption, were computed. An experimentally feasible lean methane mixture, 1.0% CH_4−4.0% O_2−95.0% Ar, $\phi = 0.5$, at $T = 1650$ K and $\rho = 33.0$ μmol cm^{-3}, suffers from large sensitivities for pyrolytic reactions such as $CH_3 + H (+M) = CH_4 (+M)$, $CH_4 + H = CH_3 + H_2$, $CH_3 + CH_3 (+M) = C_2H_6 (+M)$, and $CH_3 + CH_3 = C_2H_5 + H$. The sensitivities to pyrolytic reactions can be reduced by reducing the equivalence ratio, by reducing the mixture strength, or by increasing the rate of the title reaction. Reducing both the equivalence ratio and the mixture strength results in acceptable sensitivity values for the title reaction with respect to the secondary reactions, not true chemical isolation but a situation not entirely dissimilar. Thus, very lean mixtures were chosen for our diagnostics. Parts a and b of Figure 1 show the sensitivity spectra of t_{A50} and t_{ABS50} (defined in Results below) for the 0.5% CH_4−10.0% O_2−89.5% Ar mixture at $T = 1650$ K and $\rho = 16.5$ μmol cm^{-3} for each of the two diagnostics. First-order sensitivities for all the reactions were obtained; for clarity of presentation only those reactions with significant sensitivity are shown. The title reaction exhibits the largest sensitivity under this condition, although not the clear dominance exhibited in the sensitivity analysis of YWF (see their Figure 5). An advantage of the 214 nm diagnostic is that it lacks sensitivity to the reaction $CHO + O_2 = CO + HO_2$ that appears for the 310 nm diagnostic. To find a suitable experimental temperature range, sensitivity analyses for t_{A50} and t_{ABS50} were performed at $T = 1500$, 1650, and 1800 K, and $\rho = 16.5$ μmol cm^{-3} for 0.5% CH_4−10.0% O_2−89.5% Ar mixture (parts a and b of Figure 2, respectively). As seen in the figures, at low temperature (1500 K) the title reaction shows a dominant sensitivity for both diagnostics. However, the influence of the reactions $CH_3 + CH_3 (+M) = C_2H_6 (+M)$ and $CH_3 + HO_2 = CH_4 + O_2$ increases as temperature decreases. At high temperature (1800 K), the importance of the title reaction is decreased while that of the $CH_3 + H (+M) = CH_4 (+M)$ reaction is increased. Therefore, we chose to limit the suitable temperature range for experiments using this mixture to 1500−1800 K. Similar sensitivity spectra were obtained for other trial mixtures, leading us to select the following mixtures to use in our study: 0.4% CH_4−20.0% O_2−79.6% Ar (ϕ = 0.04), 1.0% CH_4−20.0% O_2−79.0% Ar ($\phi = 0.1$), and 0.5% CH_4−10.0% O_2−89.5% Ar ($\phi = 0.1$). Of course, one can find conditions where chemical isolation is attainable over broader temperature ranges; however, we found those conditions to suffer from overriding experimental inconvenience due to extreme time scales and absorbance for our experimental apparatus.

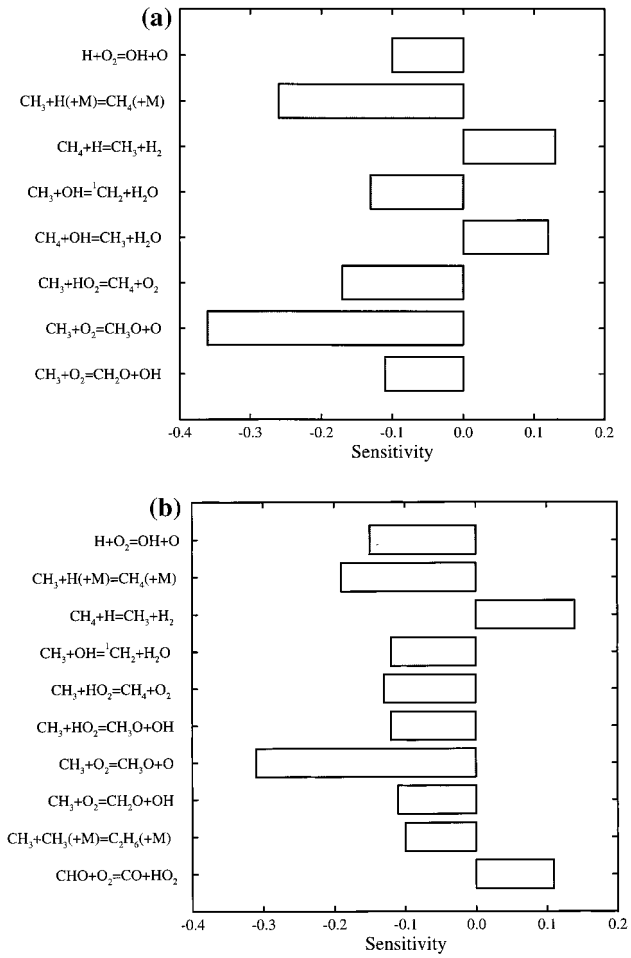

Figure 1. Logarithmic sensitivity for 0.5% CH_4−10.0% O_2−89.5% Ar mixture at $T = 1650$ K and $\rho = 16.5$ μmol cm^{-3}: (a) for 214 nm diagnostic (CH_3 absorption); (b) for 310 nm diagnostic (OH absorbance).

Results

Typical 214 and 310 nm absorption profiles are shown in parts a and b of Figure 3, respectively. The 214 nm absorption profile exhibits an initial rapid rise at shock passage due to the temperature-dependent absorption of molecular oxygen. The subsequent rise is almost entirely due to the buildup of methyl radical, which peaks immediately before the maximum pressure rise. The sudden fall of absorption signal after the peak indicates the fast consumption of CH_3 by reactive radicals, i.e., ignition. The slow rise in the postignition period is due to the formation of CO_2. In the 310 nm absorbance profile, the reflected shock passage at time zero is shown in the form of a schlieren peak. After an induction period the absorption increases rapidly because of the exponential growth of OH concentration by chain-branching reactions. After attaining a broad peak, the absorption slowly diminishes as the OH radicals seek their equilibrium concentration from the peak of the kinetic overshoot. In all mixtures intense absorption was observed if the laser was tuned to the OH line center. A series of experiments were performed with the laser tuned off line center to ensure absorbance below 0.5 at the peak.

Data reduction was accomplished by taking sets of relevant information derived from the experimental traces. We chose

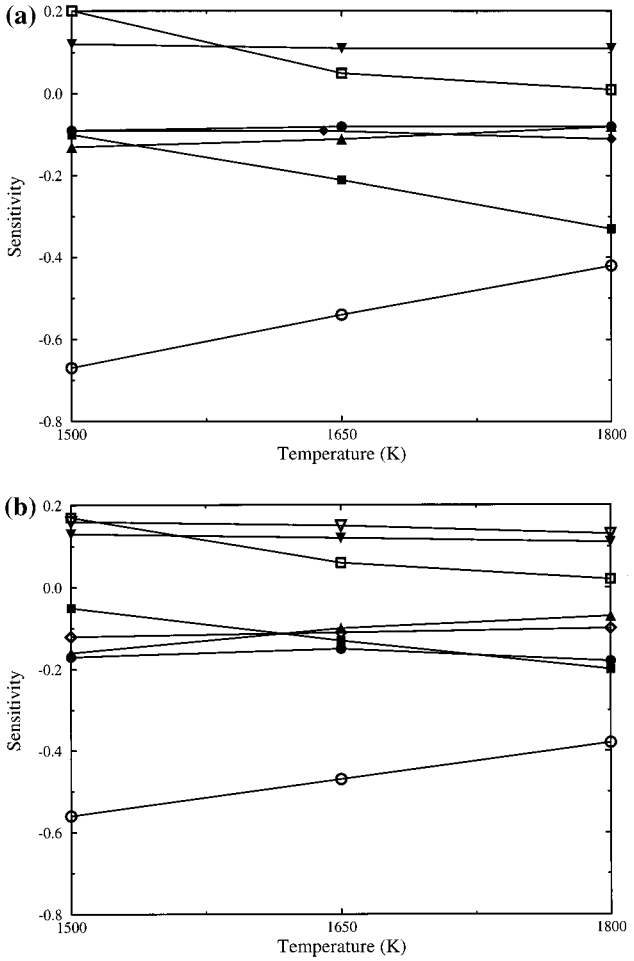

Figure 2. Logarithmic sensitivity spectra (experimental conditions are as in Figure 1): (a) for 214 nm diagnostic (CH_3 absorption); (b) for 310 nm diagnostic (OH absorbance). Symbols are for the following: filled circle, $H + O_2 = OH + O$; filled square, $CH_3 + H (+M) = CH_4 (+M)$; filled triangle down, $CH_4 + H = CH_3 + H_2$; filled diamond, $CH_3 + OH = {}^1CH_2 + H_2O$; filled triangle up, $CH_3 + HO_2 = CH_4 + O_2$; open circle, $CH_3 + O_2 = CH_3O + O$; open square, $CH_3 + CH_3 (+M) = C_2H_6 (+M)$; open diamond, $CHO + M = CO + H + M$; open triangle down, $CHO + O_2 = CO + HO_2$.

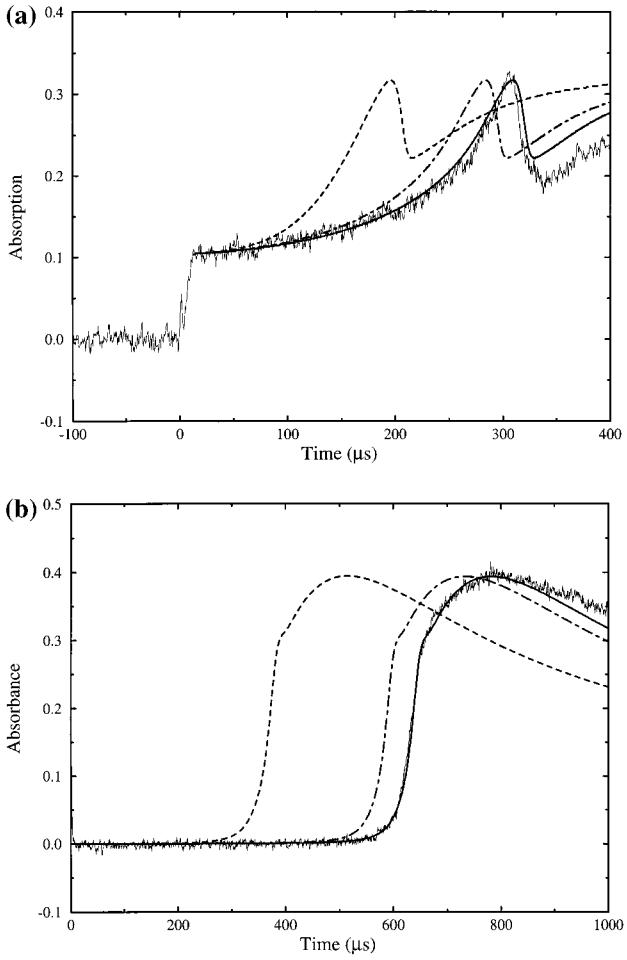

Figure 3. Typical experimental profiles: (a) for 214 nm diagnostic (CH_3 absorption), 1.0% CH_4−20.0% O_2−79.0% Ar, $T = 1593$ K, and $\rho = 19.5$ μmol cm^{-3}; (b) for 310 nm diagnostic (OH absorbance), 0.5% CH_4−10.0% O_2−89.5% Ar, $T = 1594$ K and $\rho = 16.4$ μmol cm^{-3}. Smooth lines are from simulations using GRI_MECH, version 2.11, with the following choices for $k(CH_3 + O_2 = CH_3O + O)$: solid line, present study; dot−dashed line, present study increased by 30% (upper uncertainty bound); dashed line, GRI_MECH, version 2.11, value.

characteristic times based on either the maximum absorption, A_{max}, or the maximum absorbance, ABS_{max}. For the 214 nm diagnostic t_{Amax}, t_{A75}, t_{A50}, and t_{A25} were chosen, where these are the elapsed times required to reach 100%, 75%, 50%, and 25% of A_{max} (a correction was applied for the initial absorption due to molecular oxygen). For the 310 nm diagnostic characteristic times, t_{ABS75}, t_{ABS50}, and t_{ABS25} were chosen, where these are the elapsed times required to reach 75%, 50%, and 25% of maximum absorbance. Measurements of these characteristics were unaffected by the choice of laser wavelength, either tuned on or off the OH line center. Both absorption and absorbance are obtained via straightforward arithmetical operation from the raw experimental trace. The choice between them for use in data reduction is simply a matter of personal taste. The observables we have chosen contain sufficient information content to determine the rate coefficient of the title reaction via computer simulation.

Experimental conditions, measured observables, and the rate coefficients determined for individual experiments are given in Tables 1 and 2. Three fuel lean mixtures were used for the 214 nm experiments, namely, 0.4% CH_4−20.0% O_2−79.6% Ar, 1.0% CH_4−20.0% O_2−79.0% Ar, and 0.5% CH_4−10.0% O_2−89.5% Ar. For the 310 nm experiments a 0.5% CH_4−10.0% O_2−89.5% Ar mixture was used at two different densities ($\rho_{ave} = 16.5$ and 27.1 μmol cm^{-3}). Corrected temperatures for the reflected shock wave−boundary layer interaction were always higher than the ideal shock temperatures. The percent correction varied from 1.0% to 1.4% depending on mixture composition and initial test gas pressure.

Shown in Figure 4 are the t_{A50} values for the low-density 0.5% CH_4−10.0% O_2−89.5% Ar mixture measured using the 214 nm diagnostic. The scatter was caused by a somewhat large density difference between the individual experiments. Shown in Figure 5 are the t_{ABS50} values for the 0.5% CH_4−10% O_2−89.5% Ar mixture measured using the 310 nm diagnostic. We compare our t_{ABS50} measurements with those of YWF, where the same mixture and experimental technique were used. The t_{ABS50} values of the high-density ($\rho_{ave} = 15.9$ μmol cm^{-3}) measurements of YWF are smaller than our values at a comparable density ($\rho_{ave} = 16.5$ μmol cm^{-3}). Nonetheless the agreement is reasonable. Applying a temperature correction, equal to the average temperature correction for our runs, to each data point of YWF resulted in a small temperature displacement and an improvement in the agreement between the two sets of data. We disagree with YWF as to the absorption coefficients of OH for the $P_1(5)$ line of the (0,0) band of the $A^2\Sigma^+ - X^2\Pi$ transition. Use of this particular line is common to both YWF

TABLE 1: Experimental Conditions and Results of 214 nm Absorption[a]

T_5	ρ_5	P_5	t_{A25}	t_{A50}	t_{A75}	t_{Amax}	$k/10^9$
		0.4% CH_4−20.0% O_2−79.6% Ar					
1595	19.4	2.545	200	257	287	328	0.885
1634	19.7	2.639	139	183	211	241	1.15
1662	19.8	2.700	113	143	167	189	1.44
1669	19.8	2.715	103	138	157	183	1.45
1672	19.8	2.721	111	138	159	170	1.40
1683	19.9	2.754	103	127	142	158	1.49
1703	20.2	2.823	90	113	124	140	1.42
1717	20.3	2.856	78	97	112	126	1.80
1730	16.9	2.403	77	100	117	137	2.10
1742	19.1	2.736	62	83	97	110	2.19
1759	20.5	2.955	45	67	80	95	2.42
1772	20.5	2.982	55	65	73	86	2.48
1804	20.9	3.097	37	52	63	74	2.90
		1.0% CH_4−20.0% O_2−79.0% Ar					
1575	19.4	2.506	239	314	343	365	0.726
1593	19.5	2.550	205	263	289	308	0.861
1597	19.3	2.534	184	247	273	296	0.949
1607	19.6	2.578	179	229	250	268	0.984
1629	19.7	2.634	147	193	212	228	1.04
1630	19.7	2.640	145	177	199	215	1.27
1653	19.9	2.695	118	153	172	189	1.34
1671	20.1	2.756	105	132	147	157	1.37
1679	20.1	2.773	93	130	143	155	1.34
1700	20.3	2.832	92	113	122	132	1.31
1727	20.5	2.904	67	86	95	102	1.71
1728	20.5	2.904	69	67	96	104	1.78
1729	20.9	2.962	63	84	94	101	1.68
1781	20.8	3.041	42	56	65	71	2.20
1822	21.5	3.216	32	42	48	52	2.59
		0.5% CH_4−10. 0% O_2−89.5 % Ar					
1597	19.9	2.613	319	432	480	528	0.712
1603	35.1	4.618	180	255	290	317	0.726
1619	18.3	2.425	250	374	430	473	0.883
1619	35.6	4.734	149	216	246	271	0.833
1626	36.0	4.809	141	194	225	246	0.949
1630	22.6	3.028	214	289	320	352	0.894
1642	33.0	4.442	131	184	208	230	1.04
1648	34.1	4.617	114	173	198	215	1.00
1686	23.1	3.198	105	165	195	217	1.38
1729	15.7	2.232	96	156	187	209	1.97
1731	17.9	2.537	85	144	170	191	1.70
1740	23.4	3.347	77	114	129	143	1.60
1756	23.6	3.399	63	96	112	126	1.80
1796	23.9	3.515	43	67	82	92	2.42

[a] Units are K for T_5, μmol cm^{-3} for ρ_5, atm for P_5, μs for t_{A25}, t_{A50}, t_{A75}, and t_{Amax}, and cm^3 mol^{-1} s^{-1} for k.

TABLE 2: Experimental Conditions and Results of 310 nm Absorbance[a]

T_5	ρ_5	P_5	t_{ABS25}	t_{ABS50}	t_{ABS75}	$k/10^9$
		0.5% CH_4−10.0% O_2−89.5% Ar				
1594	16.4	2.145	619	637	657	0.754
1623	16.6	2.207	475	488	501	0.974
1625	16.5	2.204	481	495	512	0.892
1631	16.5	2.212	453	467	478	0.963
1632	16.5	2.208	446	460	474	1.00
1643	16.8	2.269	412	424	436	0.983
1645	16.7	2.252	405	418	433	1.03
1650	16.6	2.245	409	423	437	0.877
1654	16.7	2.264	386	398	411	1.00
		0.5% CH_4−10.0% O_2−89.5% Ar				
1656	16.7	2.265	388	399	410	0.954
1671	16.7	2.291	317	327	337	1.38
1675	16.8	2.306	332	343	356	1.04
1679	16.8	2.314	290	299	310	1.53
1683	17.1	2.356	298	307	317	1.26
1690	15.0	2.076	303	312	322	1.49
1690	16.9	2.342	296	306	315	1.13
1695	16.2	2.258	283	293	308	1.35
1700	15.2	2.114	274	284	295	1.64
1700	16.1	2.250	273	282	297	1.41
1706	16.9	2.371	254	263	271	1.36
1726	16.1	2.276	241	249	261	1.29
1730	16.7	2.376	207	215	223	1.77
1740	15.8	2.255	204	213	233	1.82
1748	16.4	2.358	187	194	200	1.88
1752	17.2	2.466	183	190	196	1.74
1759	16.2	2.340	179	186	193	1.80
1759	16.3	2.349	180	188	196	1.76
1769	16.5	2.400	157	163	169	2.34
1775	16.3	2.367	156	163	173	2.12
1775	16.3	2.379	157	163	169	2.06
1779	16.7	2.441	153	162	175	1.86
1780	16.0	2.337	151	158	164	2.27
1785	17.5	2.556	143	149	154	1.96
1807	16.1	2.382	124	129	135	2.71
1811	17.6	2.617	114	119	123	2.69
1613	28.4	3.760	353	363	371	0.700
1618	27.4	3.635	330	340	348	0.877
1620	26.7	3.551	359	336	344	0.935
1668	25.9	3.543	232	239	251	1.17
1696	26.1	3.631	176	188	197	1.46

[a] Units are K for T_5, μmol cm^{-3} for ρ_5, atm for P_5, μs for t_{ABS25}, t_{ABS50}, and t_{ABS75}, and cm^3 mol^{-1} s^{-1} for k.

and the present study. In fact, the two laser−detector systems are nearly identical. However, the absorption coefficients derived from YWF expression were about one-third of our values. As stated previously, we tuned off line center to limit absorbance below 0.5 OD and we took great care to ensure linear optical response.

Previously, sensitivity spectra versus experimental observables (t_{A50} or t_{ABS50}) at a typical condition for different diagnostics were shown. However, in deriving the target parameter (rate coefficient), one must consider the effect of other assumed reaction rate coefficients on the target parameter through the experimental observables. This cross sensitivity was computed for each of the diagnostics used; for the 0.5% CH_4−10.0% O_2−89.5% Ar mixture, the reactions $H + O_2 = OH + O$ and $CH_3 + H (+M) = CH_4 (+M)$ showed the largest cross sensitivities. The rate coefficient of the CH_4 decomposition reaction was found to be very important in determining k values of the title reaction at high temperatures. Similar results were obtained with the other mixtures. Since the reaction $H + O_2 = OH + O$ is well-known, the difference between recent studies being about 10%,[37−40] we checked only the CH_4 decomposition rate coefficient expression of GRI_MECH, version 2.11 by performing a separate set of experiments. Our findings are that while the reaction is not in the low-pressure limit for our conditions, the rate coefficients for our conditions are almost identical to those generated by GRI_MECH, version 2.11.[41] We believe that there is no overwhelming bias due to cross sensitivities of the other reaction rate coefficients used in our determination. This is not to say that we were unaffected by secondary chemistry (of which more later).

Very lean CH_4−O_2−Ar mixtures ($\phi = 0.04$ and 0.1) were used in the present study, and so the effect of vibrational relaxation times on the data reduction must be examined. The vibrational relaxation of O_2 predominates in our experiments. A mixture rule, $(1/(p\tau))_{mixture} = \sum x_i/(p\tau_{O2-i})$, was used for the calculation of vibrational relaxation time, where τ is the vibrational relaxation time of the system, x_i is the mole fraction of species i in the mixture, τ_{O2-i} is the relaxation time of O_2 infinitely diluted in i, and p is the total pressure of the system. The τ_{O2-O2} and the τ_{O2-Ar} were computed using the Landau−Teller type formulas of Millikan and White.[42] The rate of the intermolecular V−T energy transfer between O_2 and CH_4 was

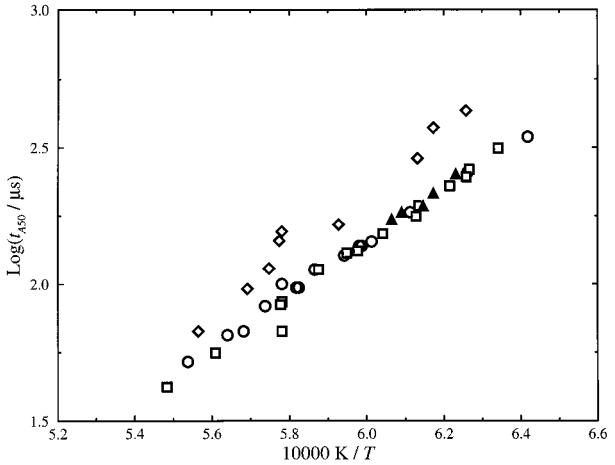

Figure 4. t_{A50} vs $1/T$ (214 nm, CH_3 absorption). Symbols are for the following: open circle, 0.4% CH_4−20.0% O_2−79.6% Ar, $\rho_{ave} = 19.7$ μmol cm^{-3}; open square, 1.0% CH_4−20.0% O_2−79.0% Ar, $\rho_{ave} = 20.1$ μmol cm^{-3}; filled triangle up, 0.5% CH_4−10.0% O_2−89.5% Ar, $\rho_{ave} = 34.8$ μmol cm^{-3}; open diamond, 0.5% CH_4−10.0% O_2−89.5% Ar, $\rho_{ave} = 20.9$ μmol cm^{-3}.

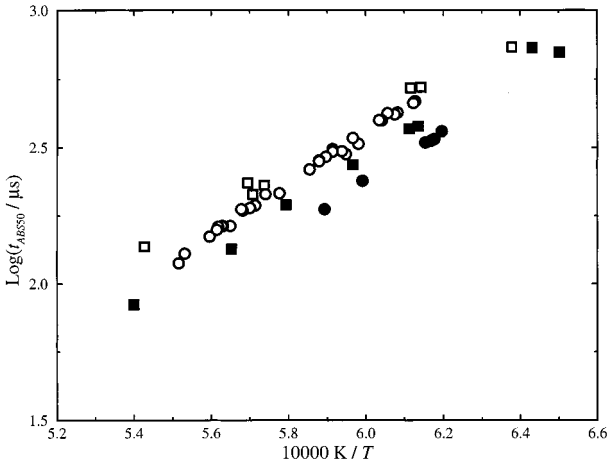

Figure 5. t_{ABS50} vs $1/T$ (310 nm, OH absorbance) for 0.5% CH_4−10.0% O_2−89.5% Ar mixture. Symbols are for the following: open circle, present study, $\rho_{ave} = 16.5$ μmol cm^{-3}; filled circle, present study, $\rho_{ave} = 27.1$ μmol cm^{-3}; open square, YWF, $\rho_{ave} = 10.8$ μmol cm^{-3}; filled square, YWF, $\rho_{ave} = 15.9$ μmol cm^{-3}.

calculated by Jones et al.[43,44] based on the theory of Schwartz, Slawsky, and Herzfeld. The computed collision number for one quantum of energy transfer in O_2 by CH_4 at 296 K was 5.61×10^6, while that by O_2 was 8.31×10^7. With these collision numbers and σ_{O2-O2} and σ_{O2-CH4} obtained assuming Lennard-Jones 12-6 potential,[45] the ratio of vibrational relaxation times, $\tau_{O2-CH4}/\tau_{O2-O2}$ is about 0.1. The τ_{O2-CH4} values were calculated by assuming that τ_{O2-CH4} has the same temperature dependence ($T^{-1/3}$) and mass effect (reduced mass μ) as τ_{O2-O2} and then were reduced by the ratio shown above. The total system relaxation times (τ) calculated in this way under our experimental conditions ranged from 5 to 15 μs. The ratio, t_{A50}/τ or t_{ABS50}/τ ranged from 10 to 40. We therefore conclude that vibrational relaxation of O_2 did not affect our data reduction.

A modeling study was performed using the mechanism mentioned above and the characteristic times (t_{Amax}, t_{A75}, t_{A50}, and t_{A25}; t_{ABS75}, t_{ABS50}, and t_{ABS25}) as target criteria. In the simulation only the rate coefficient of the title reaction was varied. The rate coefficients so determined are entered in the last columns of Tables 1 and 2 and also plotted in Figure 6. When the characteristic times were matchedm very good

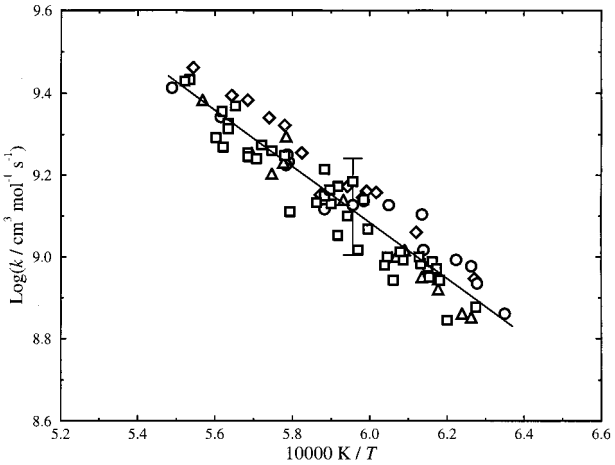

Figure 6. Arrhenius plot of the experimental data for $k(CH_3 + O_2 = CH_3O + O)$. The solid line is the least-squares fit to the data; $k = 1.60 \times 10^{13}$ exp(−15813 K/T) cm^3 mol^{-1} s^{-1} (1575 K ≤ T ≤ 1822 K). Symbols are for the following: open diamond, open circle, and open triangle up for 214 nm diagnostic (CH_3 absorption); open square for 310 nm diagnostic (OH absorbance). The error bar represents a conservative estimation of errors (±30%) in individual measurement.

agreement with the entire experimental profile was obtained. A least-squares fit of our rate coefficients to the Arrhenius expression gives

$$k = (1.60^{+0.67}_{-0.47}) \times 10^{13} \exp(-15813 \pm 587\ \mathrm{K}/T)\ \mathrm{cm^3\,mol^{-1}\,s^{-1}}$$

with a 13% standard deviation, in the temperature range 1575−1822 K.

An error analysis was performed for the experimental determinations of k. By use of the known uncertainty contributions for our measurement equipment and estimates of the uncertainty contributions from the shock velocity, the characteristic time (t_{A50} or t_{ABS50}), P_5 (used in the temperature correction), and the level of pure O_2 absorption, the overall uncertainty for a series of typical experimental conditions was computed. The individual uncertainty contributions are 3% and 4% derived from a 0.1 μs uncertainty in time measurement for the calculation of shock velocity, 15% and 22% from a 1% uncertainty in P_5 measurement used in the temperature correction and 6% from a 2% uncertainty in characteristic time (t_{A50} or t_{ABS50}) measurement for 214 and 310 nm experiments, respectively. For the 214 nm experiments an additional uncertainty in the characteristic time (t_{A50}) due to uncertainty in locating the initial pure O_2 absorption was considered. A maximum uncertainty of 30% was calculated for both cases using the formula $U = (\sum U_i^2)^{1/2}$ (this is slightly greater than our maximum point-to-point scatter). The least-squares fit line and the uncertainty bar at the middle of the $1/T$ range are shown in Figure 6.

Discussion

We compare our results with those of previous studies in Figure 7. As can be seen, our results are clearly continuing the trend toward lower values of the rate coefficient. Those evaluations that have returned the highest values are also those that have used the most complex chemical systems. A persuasive argument that those studies were affected by that complexity has been made by YWF, but it does bear a brief repetition. Either underestimation of the extent of secondary reaction influence or, equivalently, overestimation of the extent of chemical

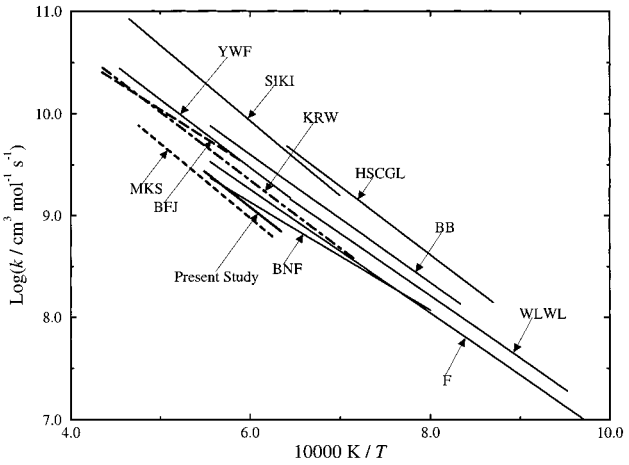

Figure 7. Comparison of the present results for $k(CH_3 + O_2 = CH_3O + O)$ to other experimental studies. Lines are for the following: BB, ref 13; BFJ, ref 15; BNF, ref 24; F, ref 19; HSCGL, ref 16; KRW, ref 20; MKS, ref 66; SIKI, ref 17; WLWL, ref 18; YWF, ref 23.

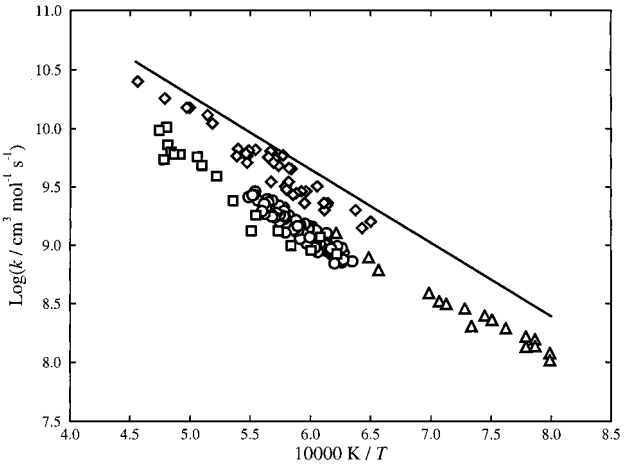

Figure 8. Comparison of the present results for $k(CH_3 + O_2 = CH_3O + O)$ to the recent experimental and modeling studies. Symbols are for the following: circle for present study; square for MKS;[66] triangle for BNF;[24] diamond for YWF;[23] solid line for GRI[35] (their optimized rate coefficient expression).

isolation achieved results in a speciously high value of the rate coefficient. We will limit our discussion to the three most recent measurements. The reported data for those three studies along with our data and the GRI_MECH, version 2.11, rate coefficient expression values are shown in Figure 8.

Our rate coefficient expression has nearly the same temperature dependence as YWF, but our pre-exponential factor is about 2.5 times lower. Of the YWF mixtures the 0.5% CH_4−10.0% O_2−89.5% Ar mixture showed the best sensitivity for the title reaction. We also chose this mixture, and a comparison of the t_{ABS50} values is shown in Figure 5. We used the same mixture, diagnostic, and almost the same experimental conditions of YWF, and so it is not surprising that our data are in good agreement. Therefore, it might appear surprising that our rate coefficient expressions are not. However, there are two reasons why this is so. The first is the result of the effect of thermochemistry and secondary chemistry, and the second has to do with how we calculate the reflected shock conditions.

The thermochemistry of CH_3O was discussed by YWF. The $\Delta_f H°_{298}(CH_3O)$ of GRI_thermodynamic data, version 2.11, is 16.3 kJ mol^{-1}, while NASA thermodynamic data[36] adopted 13.0 kJ mol^{-1} from Gurvich et al.[46] YWF used the $\Delta_f H°_{298}$ value of 12.2 kJ mol^{-1} reported by Kuo et al.[47] This value is only 0.8 kJ mol^{-1} lower than the value NASA accepted. We do agree with the conclusion of YWF that changing the value of $\Delta_f H°_{298}(CH_3O)$ has no effect on the simulation. The real effect is due to the choice of entropy values, which differ significantly between GRI and NASA. For example, at 1650 K the values of entropy of CH_3O are 339.1 and 346.9 J mol^{-1} K^{-1} from GRI and NASA, respectively, the NASA value being 7.8 J mol^{-1} K^{-1} higher. Vibrational frequencies and structural information from Foster et al.[48] were used in developing the NASA thermodynamics. Using the GRI thermodynamics and reanalyzing the experimental data result in a reduction in the apparent rate coefficient of the title reaction of about 17% at 1650 K. Even though the equilibrium constant for the title reaction calculated using the GRI entropy values is about 2.3 times smaller at 1650 K than that calculated using the NASA entropy values, it is not this reaction that is responsible for the 17% reduction in the rate coefficient. Indeed, making the title reaction irreversible has no effect. The effect is instead due to secondary chemistry; specifically, it is the influence of the choice of entropy values upon the determination of the rate of the unimolecular decomposition of CH_3O. In GRI_MECH, version 2.11, adopted for use in the present study, that reaction is written as $CH_2O + H (+M) = CH_3O (+M)$. There are ample and good reasons for writing a reaction in the exothermic rather than endothermic direction, especially when neither direction has ever been directly measured. For our experimental conditions the reaction flux actually runs in the decomposition direction and the use of GRI thermodynamics results in a rate coefficient that is about 2.5 times higher than that obtained using NASA values. In GRI_MECH, version 2.11, this reaction was estimated by analogy to the reaction $C_2H_4 + H (+M) = C_2H_5 (+M)$. There is also an expression for the CH_3O decomposition reaction estimated by Tsang and Hampson[49] that is about 1.3 times higher than the value obtained using GRI_MECH, version 2.11, and NASA thermodynamics. Use of that expression results in about a 3% reduction in the derived rate coefficient of the title reaction. Here, we have a situation where a secondary effect upon the secondary chemistry changes the derived rate coefficient by 17%; an amount larger than the 1σ scatter in our data.

It is the correction we apply to our temperature measurements, made in order to account for the boundary layer interaction, that is responsible for the bulk of the difference between the YWF and the present study. For the 0.5% CH_4−10.0% O_2−89.5% Ar mixture used in both YWF and the present study we measured an average temperature correction of 24 K. If we apply that temperature correction and make the appropriate density adjustments to the YWF data, a new set of rate coefficients may be derived by computer simulation using GRI_MECH, version 2.11, and NASA thermodynamic data. As can be seen in Figure 9 the agreement between the rate coefficients so derived and those of the present study is excellent. This is not surprising; as mentioned above, the measured characteristics in the two studies are in good agreement, and in both experiments the observation location was 12.7 mm from the end wall. The reflected shock−boundary layer interaction is a well-known gas dynamic effect[50−56] that results in the formation of the familiar "lambda" shock structure (so named because of its resemblance to the Greek letter λ). Briefly, the reflected shock is lifted away from the side walls because of a roll-up of the incident shock boundary layer resulting in a narrowing of the free stream, an increase in the temperature and pressure above the ideal shock conditions, and a clear bifurcation in the pressure signal observed at the side walls. A simple methodology to correct for this effect was developed by Michael and Sutherland, and its use and

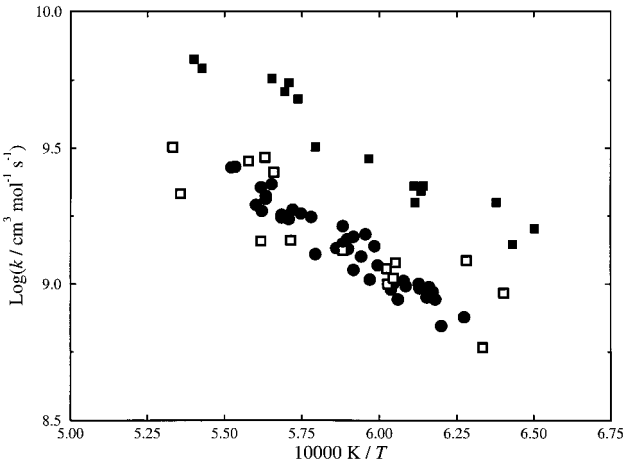

Figure 9. Comparison of our rate coefficient data with YWF results. Symbols are for the following: filled circle, present study; filled square, YWF; open square, our simulation for YWF conditions assuming a 24 K temperature correction due to the reflected shock−boundary layer interaction.

efficacy were demonstrated in a series of papers by Michael and co-workers[30,57] for dilute mixtures. The applicability of this methodology to greater mixture strengths, up to airlike stoichiometric CH_4-O_2-Ar mixtures, has been demonstrated by us previously.[40,58−62] A clear bifurcation due to the reflected shock−boundary layer interaction has also been reported by Petersen et al.[63] for CH_4-O_2-Ar mixtures (see their Figure 2).

The use of optical diagnostics necessitates that the observation location be displaced from the end wall. How much is a matter of convenience and shock tube design. Certainly the displacement must be greater than the optical beam width. Another consideration is the width of the secondary flow disturbance at the end wall.[56] For many shock tubes an offset of around 12.7 mm ($^1/_2$ in.) has been chosen. This seems like a reasonable compromise between the requirements of optical beam passage, end wall flow disturbance, and the growth of the reflected shock−boundary layer interaction strength (which increases with increasing distance from the end wall). We have observed in a separate study of methane ignition[64] that at distances below about 35 mm the temperature correction methodology is adequate and reliable. Above that distance there appears to be a coupling of the reflected shock and the reaction wave that can grow to have a dominant effect upon the course of reaction. At sufficient distance the reaction wave overtakes the reflected shock wave, and if the proper conditions are encountered, a detonation wave ensues. Shock wave−reaction wave coupling at large end wall displacement has been observed in methane combustion experiments by Brabbs and Robertson[65] and Frenklach and Bornside[6] for measurements made at 83 and 66 mm displacements, respectively.

Braun-Unkhoff et al.[24] (BNF) studied the title reaction in ultralean $CH_3N_2CH_3-O_2-Ar$ mixtures in the temperature range 1250−1600 K. BNF also used an OH laser absorption diagnostic. Their data are shown in Figure 8 as triangles. We are in good agreement with them in the limited range of mutual temperature overlap. Their extrapolated rate coefficient expression passes through the body of our data. They used an observation location that was about 5 mm from the end wall, and they did not correct the temperature for the reflected shock−boundary layer interaction. We have measured the correction at a displacement of 6.7 mm for dilute mixtures and found it to be small but not inconsequential. Since we did not use the BNF mixture or perform experiments at their end wall offset, we cannot apply the same type of reanalysis to the BNF data that we have performed for the YWF data. Application of a temperature correction to their data would improve the agreement between BNF and the present study; however, the main difference is due to the rapid recombination of methyl radicals at low temperature. Azomethane is not the clean source of methyl radicals that it would appear on first glance, especially for the study of the relatively slow $CH_3 + O_2$ reaction. For the condition shown in Figures 5−7 of their paper the initial rate of methyl recombination is 20 times faster than the rate of both $CH_3 + O_2$ channels combined. For the BNF condition the rates become equal at approximately 200 μs, a time when OH production is dominated by reactions between O_2 and secondary radicals. Examination of their Figures 5 and 6 reveals that they experience greater sensitivity to methyl recombination than to oxidation. For the low-temperature BNF condition almost all of the methyl radical recombines and is oxidized via C_2 reaction chemistry—reaction chemistry not included in the truncated BNF mechanism. Thus, the relatively high rate coefficient that BNF assign to each of the oxidation channels is, in part, a result of their assumption of a much greater degree of chemical isolation than they achieved at low temperature. At the upper end of the BNF temperature range, where they overlap the temperature range of the present study, the situation is quite different. There, the relative rates of the methyl recombination and oxidation reactions are reversed and the sensitivity to the title reaction is significantly enhanced. The rate coefficient expression that they derived for the $CH_2O + OH$ channel is nearly identical to the one used in the present study.

Michael et al.[66] (MKS) studied the title reaction in lean CH_3I-O_2-Kr mixtures in the temperature range 1600−2100 K and used an O atom ARAS diagnostic. Their data are shown in Figure 8 as squares. We are in good agreement with them in the range of mutual temperature overlap, and their rate coefficient expression, which is about 20% lower than ours, passes through the body of our data. MKS applied a correction to their measured temperatures using a methodology similar to ours. The MKS experiment is not sensitive to the CH_3O decomposition reaction, although it is sensitive to the rate of the reaction $CH_2O + O_2 = CHO + HO_2$. MKS argue that there is no reaction flux through the $CH_2O + OH$ channel. In a limited optimization of the branching ratio of the $CH_3 + O_2$ reaction we were able to reduce the $CH_2O + OH$ channel by a factor of 3 while keeping the target criteria within our experimental uncertainty. The $CH_3O + O$ channel always remained within the 30% uncertainty bounds of the value determined above (see Results above). We were unable to reduce the $CH_2O + OH$ channel to the zero flux of MKS. This, however, is a result of the limited nature of our exercise and the inadequate scope of our data for such a task, and so we have no basis to question the GRI_MECH, version 2.11, expression for the $CH_2O + OH$ channel. We believe that in the future coordinated studies will be needed in which different diagnostic techniques and mixture compositions are used in order to provide sufficient and reliable data for the optimization of the branching ratio. This was not the aim of the present study.

BNF, MKS, and the present study are in reasonably good agreement on the reported values of the rate coefficient of the title reaction. The three studies do disagree on the secondary chemistry, principally on the rate coefficient of the $CH_2O + OH$ channel. We agree with the argument of MKS that the use of OH temporal profile matching makes decoupling the two reaction channels difficult. However, we believe that the two channels are stubbornly linked, and no study to date has been

able to untwine them. We cannot eliminate the $CH_2O + OH$ channel as MKS proposes and still match either our OH or CH_3 temporal profiles. In a continuance of the normal chain of events, reducing or removing one reaction channel just brings another, usually unmeasured, reaction or set of reactions into play. This is the case in the present study where CH_3O decomposition comes to the fore. In other studies it has been other reactions or reaction pathways.[67] Ultimately, the fuel is oxidized.

All recent determinations of the title reaction have returned rate coefficients considerably below the GRI_MECH, version 2.11, value as is readily apparent from casual examination of Figure 8. When evaluated at 1600 K, there has been a monotonic decrease in the rate coefficient for the most recent studies. No group has achieved chemical isolation. We freely admit that we have not achieved chemical isolation in the present study. It is the growing appreciation of the effects of secondary reaction chemistry that has led us and others to perform more carefully designed experiments and more critical analysis. This, in turn, has led to lower rate coefficients for the title reaction. We believe that improved understanding of the secondary reaction chemistry and clarification of the relevant thermochemistry will serve to lower the rate coefficient further.

Conclusions

The rate coefficients for the reaction $CH_3 + O_2 = CH_3O + O$ were determined in a series of experiments run behind reflected shock waves. Three different mixtures and two different diagnostics were used. Modeling analysis of the results yielded an Arrhenius rate coefficient expression

$$k = (1.60\ ^{+0.67}_{-0.47}) \times 10^{13} \exp(-15813 \pm 587\ \mathrm{K}/T)\ \mathrm{cm^3\,mol^{-1}\,s^{-1}}$$

in the temperature range 1575−1822 K. All measurements to date, including the present study, have been to some extent affected by secondary reactions. Appreciation of the effects of these reactions upon the determination of the rate coefficient of the title reaction has been responsible for the overall decline in the reported values.

Acknowledgment. We are thankful to J. V. Michael for providing us with a prepublication version of his manuscript. S.M.H., S.O.R., and K.J.D. gratefully acknowledge the generous support of the National Aeronautics and Space Administration under Grant NAG3-1307. We also acknowledge the able assistance of A. L. Tischer in performing the methane decomposition experiments referenced in the present study.

References and Notes

(1) Seery, D. J.; Bowman, C. T. *Combust. Flame* **1970**, *14*, 37.
(2) Lifshitz, A.; Scheller, K.; Burcat, A.; Skinner, G. B. *Combust. Flame* **1971**, *16*, 311.
(3) Jachimowski, C. J. *Combust. Flame* **1974**, *23*, 233.
(4) Tsuboi, T.; Wagner, H. Gg. In *Proceedings of the Fifteenth Symposium* (*International*) *on Combustion*; The Combustion Institute: Pittsburgh, PA, 1975; p 883.
(5) Krishnan, K. S.; Ravikumar, R. *Combust. Sci. Technol.* **1981**, *24*, 239.
(6) Frenklach, M.; Bornside, D. E. *Combust. Flame* **1984**, *56*, 1.
(7) Gardiner, W. C.; Hwang, S. M.; Rabinowitz, M. J. *Energy Fuels* **1987**, *1*, 545.
(8) Frenklach, M.; Wang, H.; Rabinowitz, M. J. *Prog. Energy Combust. Sci.* **1992**, *18*, 47.
(9) Spadaccini, L. J.; Colket, M. B., III *Prog. Energy Combust. Sci.* **1994**, *20*, 431.
(10) Yang, H.; Qin, Z.; Lissianski, V.; Gardiner, W. C. *Isr. J. Chem.* **1996**, *36*, 305.
(11) Petersen, E. L.; Röhrig, M.; Davidson, D. F.; Hanson, R. K.; Bowman, C. T. In *Proceedings of the Twenty-Sixth Symposium* (*International*) *on Combustion*; The Combustion Institute: Pittsburgh, PA, 1996; p 799.
(12) Schott, G. L. *Combust. Flame* **1973**, *21*, 357.
(13) Brabbs, T. A.; Brokaw, R. S. In *Proceedings of the Fifteenth Symposium* (*International*) *on Combustion*; The Combustion Institute: Pittsburgh, PA, 1974; p 893.
(14) Westbrook, C. K.; Lund, J. C.; Dryer, F. L. *J. Phys. Chem.* **1977**, *81*, 2542.
(15) Bhaskaran, K. A.; Frank, P.; Just, Th. In *Proceedings of the 12th International Symposium on Shock Tubes and Waves*; Lifshitz, A., Rom, J., Eds.; Magnes: Jerusalem, Israel, 1980; p 503.
(16) Hsu, D. S. Y.; Shaub, W. M.; Creamer, T.; Gutman, D.; Lin, M. C. *Ber. Bunsen-Ges. Phys. Chem.* **1983**, *87*, 909.
(17) Saito, K.; Ito, R.; Kakumoto, T.; Imamura, A. *J. Phys. Chem.* **1986**, *90*, 1422.
(18) Wu, C. H.; Lin, C.-Y.; Wang, H.-T.; Lin, M. C. In *Proceedings of the 17th International Symposium on Shock Tubes and Waves*; Kim, Y. W., Ed.; American Institute of Physics: New York, 1989; p 450.
(19) Fraatz, W. Ph.D. Dissertation, Georg-August-Universität zu Göttingen, 1990.
(20) Klatt, M.; Röhrig, M.; Wagner, H. Gg. *Ber. Bunsen-Ges. Phys. Chem.* **1991**, *95*, 1163.
(21) Ohmori, K.; Yoshimura, M.; Koshi, M.; Matsui, H. *Bull. Chem. Soc. Jpn.* **1992**, *65*, 1317.
(22) Grela, M. A.; Amorebieta, V. T.; Colussi, A. J. *J. Phys. Chem.* **1992**, *96*, 7013.
(23) Yu, C.-L.; Wang, C.; Frenklach, M. *J. Phys. Chem.* **1995**, *99*, 14377.
(24) Braun-Unkhoff, M.; Naumann, C.; Frank, P. In *Proceedings of the 19th International Symposium on Shock Waves*; Brun, R., Dumitrescu, L. Z., Eds.; Springer-Verlag: Berlin, 1995; p 203.
(25) Ewig, F.; Rhäsa, D.; Zellner, R. *Ber. Bunsen-Ges. Phys. Chem.* **1987**, *91*, 708.
(26) Zellner, R.; Ewig, F. *J. Phys. Chem.* **1988**, *92*, 2971.
(27) Cobos, C. J.; Hippler, H.; Luther, K.; Ravishankara, A. R.; Troe, J. *J. Phys. Chem.* **1985**, *89*, 4332.
(28) Dean, A. M.; Westmoreland, P. R. *Int. J. Chem. Kinet.* **1987**, *19*, 207.
(29) Baldwin, A. C.; Golden, D. M. *Chem. Phys. Lett.* **1978**, *55*, 350.
(30) Michael, J. V.; Sutherland, J. W. *Int. J. Chem. Kinet.* **1986**, *18*, 409.
(31) Engstrom, R. W. In *Photomultiplier Handbook*; RCA: Lancaster, PA, 1980.
(32) Kee, R. J.; Rupley, F. M.; Miller, J. A. *Chemkin-II: A Fortran Chemical Kinetics Package for the Analysis of Gas-Phase Chemical Kinetics*; Report SAND89-8009; Sandia National Laboratories: Livermore, CA, 1989.
(33) Radhakrishnan, K. *LSENS—A General Chemical Sensitivity and Analysis Code for Homogeneous Gas-Phase Reactions*; NASA RP 1328; National Aeronautics and Space Administration: Washington, DC, 1994.
(34) Radhakrishnan, K.; Hindmarsh, A. C. *Description and Use of LSODE, The Livermore Solver for Ordinary Differential Equations*; NASA RP 1327; National Aeronautics and Space Administration: Washington, DC, 1993 (also in Lawrence Livermore National Laboratory Report UCRL-ID-113855, 1993).
(35) Frenklach, M.; Wang, H.; Yu, C.-L.; Goldenberg, M.; Bowman, C. T.; Hanson, R. K.; Davidson, D. F.; Chang, E. J.; Smith, G. P.; Golden, D. M.; Gardiner, W. C.; Lissianski, V. *GRI_MECH*, version 2.11 (http://www.me.berkeley.edu/gri_mech/). Frenklach, M.; Wang, H.; Yu, C.-L.; Goldenberg, M.; Bowman, C. T.; Hanson, R. K.; Davidson, D. F.; Chang, E. J.; Smith, G. P.; Golden, D. M.; Gardiner, W. C.; Lissianski, V. *GRI_Mech—An Optimized Detailed Chemical Reaction Mechanism for Methane Combustion*; Report No. GRI-95/0058; Gas Research Institute, 1995.
(36) McBride, B. J.; Gordon, S.; Reno, M. A. *Coefficients for Calculating Thermodynamic and Transport Properties of Individual Species*; NASA TM-4513; National Aeronautics and Space Administration: Washington, DC, 1993.
(37) Masten, D. A.; Hanson, R. K.; Bowman, C. T. *J. Phys. Chem.* **1990**, *94*, 7119.
(38) Shin, K. S.; Michael, J. V. *J. Chem. Phys.* **1991**, *95*, 262.
(39) Yu, C.-L.; Frenklach, M.; Masten, D. A.; Hanson, R. K.; Bowman, C. T. *J. Phys. Chem.* **1994**, *98*, 4770.
(40) Ryu, S.-O.; Hwang, S. M.; Rabinowitz, M. J. *J. Phys. Chem.* **1995**, *99*, 13984.
(41) Hwang, S. M.; Ryu, S.-O.; Rabinowitz, M. J. Manuscript in preparation.
(42) Millikan, R. C.; White, R. R. *J. Chem. Phys.* **1963**, *39*, 3209.
(43) Jones, G.; Lambert, J. D.; Stretton, J. L. *Proc. Phys. Soc.* **1965**, *86*, 857.
(44) Lambert, J. D. In *Vibrational and Rotational Relaxation in Gases*; Clarendon Press: Oxford, 1977; Chapter 4.

(45) Hirschfelder, J. O.; Curtiss, C. F.; Bird, R. B. In *Molecular Theory of Gases and Liquids*; Wiley: New York, 1954.

(46) Gurvich, L. V.; Veyts, I. V.; Alcock, C. B. In *Thermodynamic Properties of Individual Substances*, 4th ed.; Hemisphere Publishing Corporation: New York, 1991; Vol. 2, Part 1, p 67.

(47) Kuo, S.-C.; Zhang, Z.; Klemm, R. B.; Liebman, J. F.; Stief, L. J.; Nesbitt, F. L. *J. Phys. Chem.* **1994**, *98*, 4026.

(48) Foster, S. C.; Misra, P.; Lin, T.-Y. D.; Damo, C. P.; Carter, C. C.; Miller, T. A. *J. Phys. Chem.* **1988**, *92*, 5914.

(49) Tsang, W.; Hampson, R. F. *J. Phys. Chem. Ref. Data* **1986**, *15*, 1242.

(50) Schlichting, H. In *Boundary Layer Theory*; McGraw-Hill: New York, 1960.

(51) Mark, H. *The Interaction of Reflected Shock Wave with the Boundary Layer in a Shock Tube*; NACA TM-1418; NACA: Washington, DC, 1958.

(52) Strehlow, R. A.; Cohen, A. *J. Chem. Phys.* **1959**, *30*, 257.

(53) Sanderson, R. J. *AIAA J.* **1969**, *7*, 1370.

(54) Matsuo, K.; Kawagoe, S.; Kage, K. *Bull. JSME* **1974**, *17*, 1039.

(55) Zhilin, Yu. V.; Bazhenova, T. V.; Gvozdeva, L. G. *Arch. Mech.* **1978**, *30*, 675.

(56) Wilson, G. J.; Sharma, S. P.; Gillespie, W. D. AIAA Paper No. 93-0480, 1993.

(57) Michael, J. V.; Fisher, J. R. In *Proceedings of the 17th International Symposium on Shock Tubes and Waves*; Kim, Y. W., Ed.; American Institute of Physics: New York, 1990; p 210 and references therein.

(58) Tischer, A. L.; Ryu, S.-O.; Hwang, S. M.; Rabinowitz, M. J. 1995 Fall Meeting, Western States Section of the Combustion Institute, Stanford, CA, 1995; Paper 95F-155.

(59) Werner, A. J.; Tischer, A. L.; Hwang, S. M.; Rabinowitz, M. J. 1996 Fall Meeting, Western States Section of the Combustion Institute, Los Angeles, CA, 1996; Paper 96F-077.

(60) Tischer, A. L.; Ryu, S.-O.; Hwang, S. M.; Rabinowitz, M. J. *Twenty-Seventh Symposium* (*International*) *on Combustion*; The Combustion Institute: Pittsburgh, PA, 1998; Poster No. W1A01.

(61) Werner, A. J.; De Witt, K. J.; Hwang, S. M.; Rabinowitz, M. J. *Twenty-Seventh Symposium* (*International*) *on Combustion*; The Combustion Institute: Pittsburgh, PA, 1998; Poster No. W1F03.

(62) Werner, A. J.; De Witt, K. J.; Hwang, S. M.; Rabinowitz, M. J. Manuscript in preparation.

(63) Petersen, E. L.; Davidson, D. F.; Hanson, R. K. AIAA Paper No. 93-0480, 1993.

(64) Tischer, A. L.; Ryu, S.-O.; Hwang, S. M.; Rabinowitz, M. J. Manuscript in preparation.

(65) Brabbs. T. A.; Robertson, T. F. *Methane Oxidation Behind Reflected Shock Waves—Ignition Delay Times Measured by Pressure and Flame Band Emission*; NASA TM-87268; National Aeronautics and Space Administration: Washington, DC, 1986.

(66) Michael, J. V.; Kumaran, S. S.; Su, M.-C. *J. Phys. Chem. A* **1999**, *103*, 5942.

(67) "All the rivers flow into the sea, and yet the sea is not full; to the place where the rivers flow, there they flow once again." Solomon, *Koheles (Ecclesiastes)* 1:7.